Duan P, Toumpaniari R, Partridge S, Birch M, Genever PA, Bull SJ, Dalgarno KW, McCaskie AW, Chen J.

How cell culture conditions affect the microstructure and nanomechanical properties of extracellular matrix formed by immortalized human mesenchymal stem cells: An experimental and modelling study.

***Materials Science and Engineering: C* 2018**

DOI: https://doi.org/10.1016/j.msec.2018.03.027

Materials Science and Engineering: C, https://doi.org/10.1016/j.msec.2018.03.027

How cell culture conditions affect the microstructure and nanomechanical properties of extracellular matrix formed by immortalized human mesenchymal stem cells: an experimental and modelling study

Pengfei Duan[1], Ria Toumpaniari[1], Simon Partridge[1], Mark A Birch[2], Paul G Genever[3], Steve J Bull[1], Kenneth W Dalgarno[1], Andrew W McCaskie[2], Jinju Chen[1,*]

1. School of Engineering, Newcastle University, Newcastle upon Tyne, NE1 7RU, UK
2. Division of Trauma and Orthopaedic Surgery, University of Cambridge, Cambridge, CB2 2QQ, UK
3. Department of Biology, University of York, York, YO10 5DD, UK

(*) Corresponding author: Jinju.chen@ncl.ac.uk

Abstract

This paper presents an investigation of how different culture media (*i.e.* basal and osteogenic media) affect the nanomechanical properties and microstructure of the mineralized matrix produced by the human mesenchymal stem cell line Y201, from both an experimental and theoretical approach. A bone nodule (*i.e.* mineralized matrix) cultured from basal medium shows a more anisotropic microstructure compared to its counterpart cultured from an osteogenic medium. As confirmed by finite element simulations, this anisotropic microstructure explains the bimodal distribution of the corresponding mechanical properties very well. The overall nanomechanical response of the bone nodule from the osteogenic medium is poorer compared to its counterpart from the basal medium. The bone nodules, from both basal and osteogenic media, have shown reverse aging effects in terms of mechanical properties. These are possibly due to the fact that cell proliferation outcompetes the mineralization process.

Keywords

Nanomechanical properties; Biological materials; Finite element modelling; Mesenchymal stem cells

1. Introduction

Tissue engineering is the use of a combination of cells, biomaterials and suitable biochemical and physicochemical factors to improve or replace biological tissues. In the last decades, biomaterial scaffolds have been widely used in bone tissue engineering [1-5]. Scaffolds with various combinations of constituents are designed to achieve a better biofunctionality and mechanical strength. Of these, cell-based materials have provided exciting prospects for future exploitation [6-8]. Very recently, genetic modified cells have been adopted [9]. The immortalized cell line Y201 derived from human mesenchymal stem cells (hMSCs) circumvents the issues of limited life-span and high variability of hMSCs [10, 11]. However, whether these cells may proliferate in suitable manner and produce appropriate mineralized matrix for given cell culture conditions remains elusive, which is essential for bone regeneration.

To achieve this, it is essential to understand the properties of the mineralized matrix synthesized by these cells [3, 12-14]. Due to its inhomogeneity in both chemistry and microstructure, the nanomechanical properties of such inhomogeneous materials are difficult to be reliably measured, especially for a thin layer of mineralized matrix.

Nanoindentation has proven an effective technique to assess the nanomechanical properties of natural tissues such as bone and biological cells [15-22]. Our previous work has demonstrated that the measured apparent elastic modulus generally has a bimodal distribution and the Gaussian mixture model enabled us to extract properties for two components in the matrix [23]. However, there is a lack of comprehensive studies on how cell culture conditions would affect the new tissue formation and the mechanical properties of these new tissues. This is important for us to understand the cell-material interactions and the influence of chemical stimuli on biological processes, which will provide an invaluable guideline for scaffold material design and optimising cell culture conditions.

Therefore, in this study, we adopted nanoindentation to characterize the mechanical properties of the mineralized matrix synthesized by the immortalized cell line Y201 from hMSCs cultured in basal and osteogenic media for different periods. To reveal more insights into the nanoindentation response of these complex materials, finite element modelling was also employed.

Native mature bone always presents an aging effect in its mechanical properties [24-26]. It has been reported that there is a gradual decrease in mechanical properties (stiffness, strength, and toughness) of human femoral bone with age [25]. However, the possible aging effect of the mineralized matrix (*i.e.* early stage bone nodule) has never been reported. This is also studied in this work.

2. Materials and Methods

2.1 Sample Preparation

An immortalized hMSC line overexpressing human telomerase reverse transcriptase (hTERT) (Y201), which is a highly characterized clonal MSC line that exhibits tri-lineage differentiation capacity [9], was expanded in culture medium containing Dulbecco's modified Eagle's Medium with 10% fetal bovine serum, 20 mM Glutamax and Penicillin/Streptomycin 1,00 U/ml without further characterisation and passaged when cells reached approximate 80% confluency. An osteogenic medium containing culture medium supplemented with 50 μg/ml l-ascorbic acid, 10 mM glycerophosphate and 100 nM dexamethasone was used as comparison [27-29].

Y201 cells were trypsinized and seeded at 15,000 cells/cm^2 onto 13 mm diameter glass slides and were allowed to adhere for 4 hours. They were then cultured in basal and osteogenic media (BM and OM) for 7, 14 and 21 days. For samples cultured in the OM, the cells grow so fast that they detached from the substrate on day 21 and thus no samples were harvested from this period. The medium was replenished every three days. For each given cell culture condition, 3 samples were measured in each experiment.

In order to study the collagen fibre distribution, additional samples were demineralized by immersing the samples in an ethylenediaminetetraacetic acid (EDTA) solution (0.5 M, pH 7.4) for 6 hours to dissolve the mineral phase. After that, each sample was gently rinsed in deionized water several times to remove the EDTA [30]. The thickness of the matrix layer was measured by ball cratering (Pascall Engineering Co. Ltd., Sussex, UK). In this study, the thickness is 18.5±8.4 μm at the centre of the sample.

2.2 Surface analysis

Prior to nanomechanical tests, a ZYGO 5000 profilometer (ZYGO Corporation, Middlefield, CT, USA) was used to measure the surface roughness of the samples. The surface morphology and chemical composition were analysed by scanning electron microscopy (SEM) (HITACHI TM3030, Hitachi High-Technologies, Wokingham, UK), which was equipped with energy-dispersive X-ray spectroscopy (EDS) for elemental analysis.

Extensive research has reported that collagen fibres can be observed under polarized light microscopy due to their birefringent property [31-36]. Thus, the collagen fibre analysis of demineralized samples was performed with an Olympus BH2-UMA polarizing microscope (Olympus Europa GmbH, Hamburg, Germany).

2.3 Nanoindentation

Nanoindentation tests were performed with a Hysitron Triboindenter (Hysitron Inc., Minneapolis, MN, USA), fitted with a Berkovich diamond indenter. Measurement of the nanomechanical characteristics of mineralized matrix is challenging due to its inhomogeneity at the scale of the deforming volume, which was described in our previous preliminary work [23]. In this study, a multi-cycling test protocol with peak load varying from 1000 μN to 9000 μN was employed. This protocol enables examining the depth-dependent responses at a given location [37]. The indention tests were made at the centre of the samples. The machine stiffness and tip shape were accurately calibrated using a fused silica standard and the method of Oliver and Pharr [38]. The elastic modulus and hardness were determined by the Oliver and Pharr method [38], using

$$S = \frac{dP}{dh} = \frac{2}{\sqrt{\pi}} E_r \sqrt{A} \qquad (1)$$

$$H = \frac{P_{max}}{A} \qquad (2)$$

where *S* is the contact stiffness at peak load calculated from the slope of the upper part of the unloading curve, *P* is the indentation force, *h* is the displacement, *A* is the contact area between the tip and sample, and E_r is the reduced modulus of the material which is given by

$$\frac{1}{E_r} = \frac{1 - v_s^2}{E_s} + \frac{1 - v_t^2}{E_t} \qquad (3)$$

where *E* and *v* are elastic modulus and Poisson's ratio, respectively. The subscripts *s* and *t* stand for sample and tip. For each sample, at least 64 indents were made. Elastic modulus and hardness results were expressed as arithmetic mean values with standard deviation (SD).

2.4 Statistical analysis

To determine the significant differences in properties between different media and culture periods, two sample t-tests assuming unequal variances (α=0.05) were conducted to assess the P-value between the mechanical properties of samples cultured at different conditions. A Gaussian mixture model was adopted to separate the anisotropic mechanical properties of the mineralized matrix from the complex nanoindentation results. In this model, by assuming that the elastic modulus or hardness distribution of each individual component follows a Gaussian distribution, the probability distribution function of elastic modulus or hardness, *f(x)*, is then given by

$$f(x) = \sum_{i=1}^{m} w_i f_i(x) \quad (4)$$

$$\sum_{i=1}^{m} w_i = 1 \quad (5)$$

$$f_i(x) = N(\mu_i, \sigma_i) \quad (6)$$

where m is the number of the components, w_i and $f_i(x)$ are volume fraction and Gaussian distribution for component i, respectively. A Matlab code was written to complete this statistical analysis. Different m values have been assumed (*i.e.* 1, 2, 3…), but only m=2 gives the best fitting results. More details about the nanoindentation protocols and statistical analysis methods used here can be found in our previous work [23].

2.5 Finite element modelling

To further understand the nanoindentation responses of the mineralized matrix, finite element modelling (FEM) was employed [39, 40]. As found in our previous study [23], the distribution of apparent elastic modulus generally appeared to be bimodal. This may be attributed to transversely isotropic properties or two components with different mechanical properties. Therefore, in this study we examined these two cases by assuming a transversely isotropic material or the matrix composed of two components in the FE model. A conical tip with equivalent semi-apical angle to a Berkovich indenter was used. This is a reasonable assumption for investigating the elastic responses.

As illustrated in Fig.1a, part 1 and part 2 present (i) the transversely isotropic properties of the matrix in two perpendicular directions, or (ii) the isotropic properties of mature and immature matrix, respectively. In the former case, the elastic modulus of the transversely isotropic fibre was set as 15 GPa in the transverse direction, and 28 GPa in the longitudinal direction. In the latter case, the elastic modulus of mature and immature bone nodules was set as 28 GPa and 15 GPa, respectively. The selected elastic moduli are within the range of our experimental measurements. The Poisson's ratio in both cases was assumed to be 0.3. As illustrated in Fig.1b, different locations were indented by a conical tip with tip radius of 0.01 μm: indented on each individual part (point A, I), indented at their interface (point E), and indented at points that are 0.25 μm (point D, F), 0.5 μm (point C, G), and 1 μm (point B, H) away from the interface. For the case of indention on each individual part, the properties of the two parts were set to be the same and the indentation occurred at the centre of the model. The model was created in ABAQUS 6.13 software. As shown in Fig.1c, only half of the whole system was modelled by employing the symmetric boundary condition, a flat surface was

assumed, a frictionless contact between the indenter and the model was assumed, and the tip was modelled as a rigid body. The interface between part 1 and part 2 was assumed to be perfectly bonded. A completely fixed boundary condition was applied to the bottom of the model. A total of 48,580 linear C3D8R eight-node elements was used, with denser mesh created underneath the indenter. The height and the width of the model were sufficiently large compared to the indentation depth so that the simulated response was not significantly affected by the boundaries. Displacement control was applied to a loading-unloading protocol with a maximum indentation depth of 0.1 to 0.7 μm in each case. The elastic modulus of the model was determined from the force-displacement data generated by using the Oliver and Pharr method.

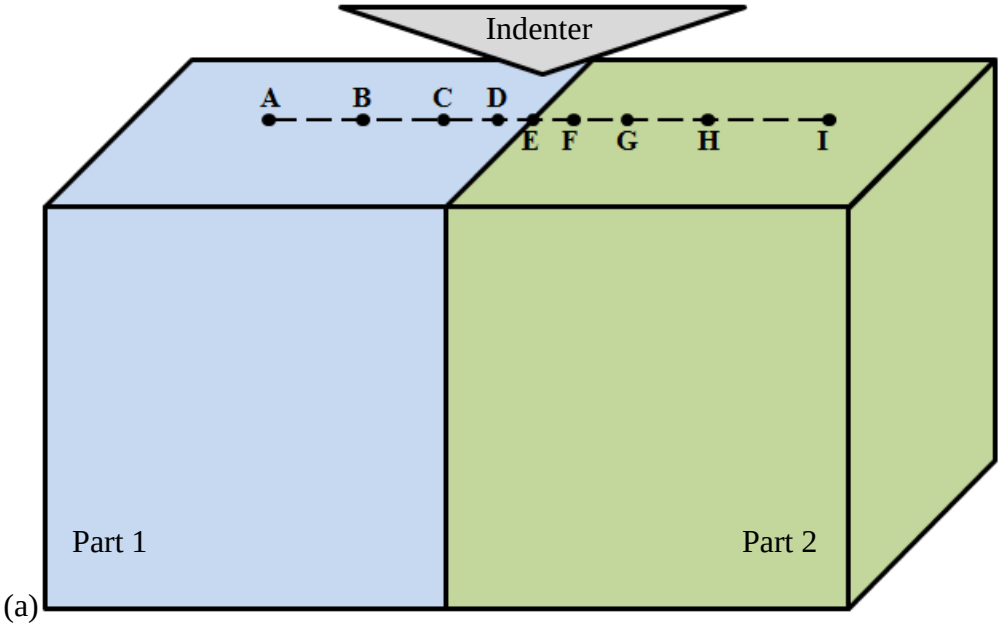

(a)

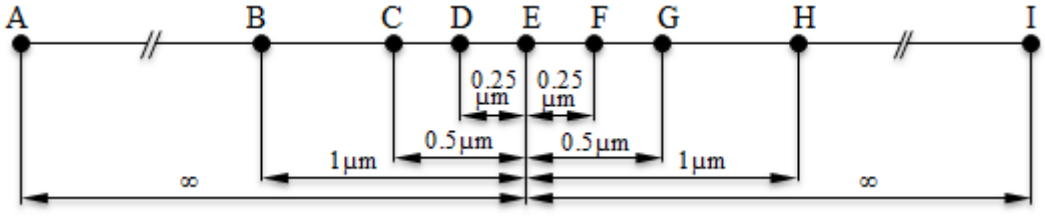

(b)

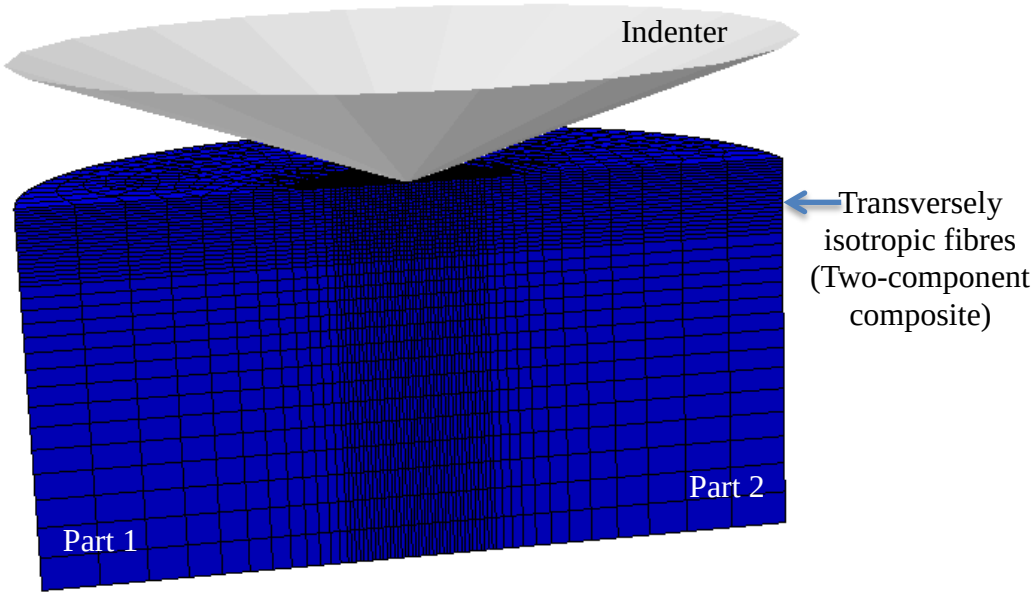

(c)

Fig.1. Schematic of (a) the model with distribution of different indented locations, (b) vertical distance of each indentation points away from the interface, and (c) the meshes for the model.

3. Results and discussion

3.1 Surface analysis

For each sample, surface roughness (the arithmetic average roughness, R_a) was measured several times at different locations near the sample centre. As shown in Table 1, the surface roughness for all the samples shows a positive correlation with the culture period for both culture media. In a fixed cell culture period, there is no significant difference between the roughness of samples cultured in BM and OM. This suggests that the surface roughness of the matrix is affected by the growth of the cells, rather than by the culture media.

Table 1. Surface roughness of the samples for different culture periods in BM and OM.

Media	Sample	Average surface roughness ± SD (nm)		
		day 7	day 14	day 21
BM	1	102.2±6.3	174.8±31.4	387±57.2
	2	108.6±17.2	204.0±34.7	215.4±23.8
	3	100.0±20.0	198.2±30.6	196.8±18.4
OM	1	115.6±16.5	192.2±21.2	-
	2	147.4±7.9	177.6±21.9	-
	3	107.6±12.7	181.0±14.2	-

Mineral particles were clearly observed on the samples cultured in BM for 21 days in SEM micrographs. The chemical composition of the observed minerals was analyzed by EDS, with the corresponding spectrum shown in Fig.2. The important characteristic of these minerals is the Ca/P ratio, as this ratio is related to the quality of bone [41-43]. The average Ca/P ratio (by weight) of these minerals is equal to 1.96±0.10; this value agrees well with the reported value (1.74-2.37) of a native femoral trabecular bone [41].

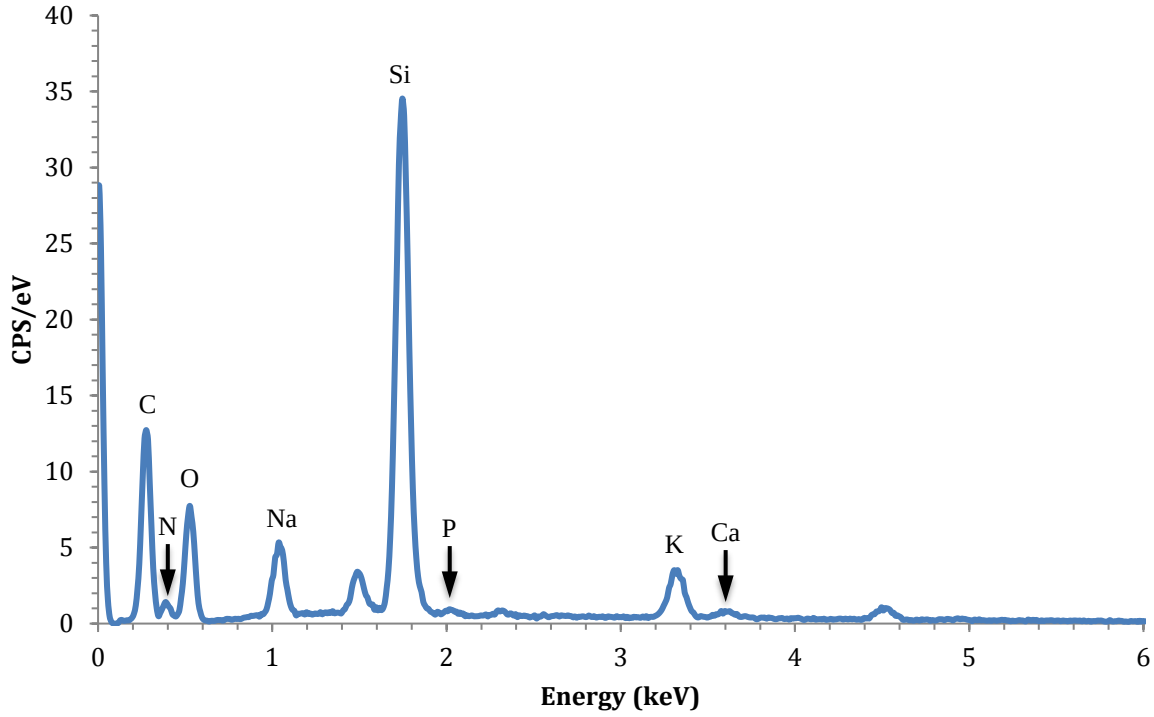

Fig.2. EDS spectrum for the minerals observed on the sample cultured in BM for 21 days.

In order to reveal more microstructural details of these extracellular matrix, polarized light images of these samples were generated. As an example, the polarized light images of samples harvested from day 14 are shown in Fig.3; collagen fibre bundles (bright spots) can be identified. They are well-aligned on the samples cultured in BM and randomly distributed on the samples cultured in OM, which suggests that the samples from BM will show anisotropic mechanical properties and the samples from OM will show relatively isotropic mechanical properties [44]. For samples harvested from day 7 and day 21, a similar observation was found.

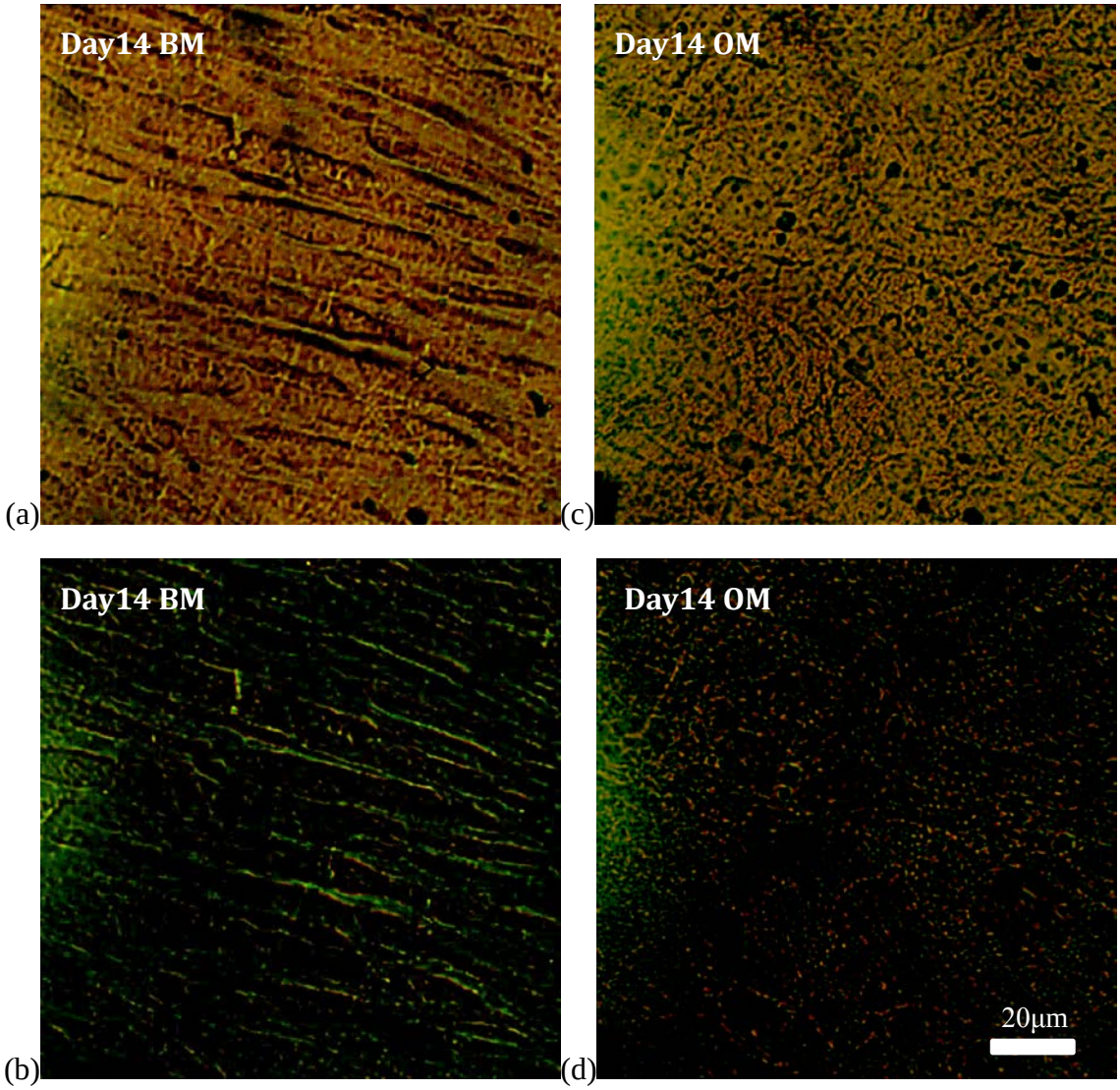

Fig.3. Representative polarized light images of samples harvested from (a, b) day 14, BM, (c, d) day 14, OM. Among them, image (a, c) are samples viewed with parallel polars, and image (b, d) are the same field viewed with crossed polars.

3.2 Nanoindentation results

3.2.1 The apparent elastic modulus and hardness

By analyzing the force-displacement curves, spatial dependent Young's modulus and hardness values were determined as a function of contact depth, as plotted in Fig.4 and Fig.5. In the given load range (1-9 mN), the average Young's modulus of samples cultured in the BM changes in the range of 18.7-27.7 GPa at day 7. These values decrease to 17.4-18.9 GPa at day 14 and 15.9-18.1 GPa at day 21. In the same load range, the average Young's modulus of samples cultured in the OM is in the range of 22.5-27.0 GPa at day 7. These values decrease to 11.1-14.2 GPa at day 14. In general, for all the samples, the measured Young's moduli decrease with the contact depth across the entire load range. Similar to the Young's moduli,

the measured hardness values also decrease with the cell culture period.

For elastic modulus, it has been reported that the modulus of collagen in nanoindentation ranges from 1.71 GPa to 3.31 GPa [45], the modulus of mouse femur is 10.76±1.61 GPa [46], and the modulus of human vertebral trabeculae is from 11.3 GPa to 15.8 GPa [47]. Thus, the elastic modulus of the matrix is similar to native bone after 7 to 14 days, and the relatively high Young's modulus of mineralized matrix in contrast to the collagen fibres indicates that the matrix is highly mineralized [45, 48]. This may suggest the matrix has a highly inhomogeneous structure near the surface. When the contact depth is below 450 nm, there is strong depth dependent behaviour for day 7 samples (both BM and OM). This indicates that the elastic modulus will be highly affected by the porous surface structure at shallow contact depth, especially for day 7 samples. With an increase of contact depth, the porous structure underneath the indenter is compressed, pores are closed up and then the corresponding elastic modulus becomes more stable.

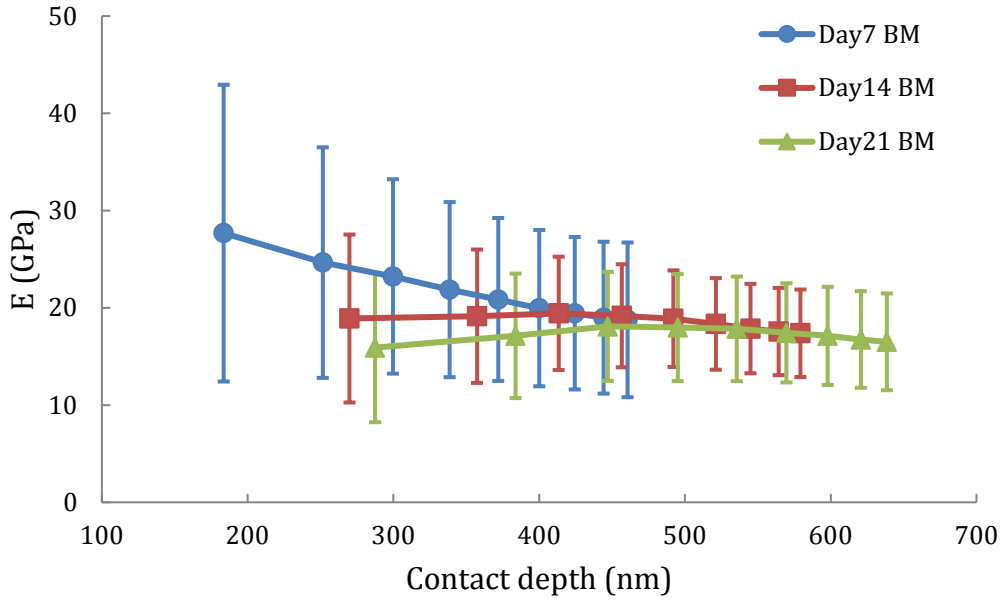

(a)

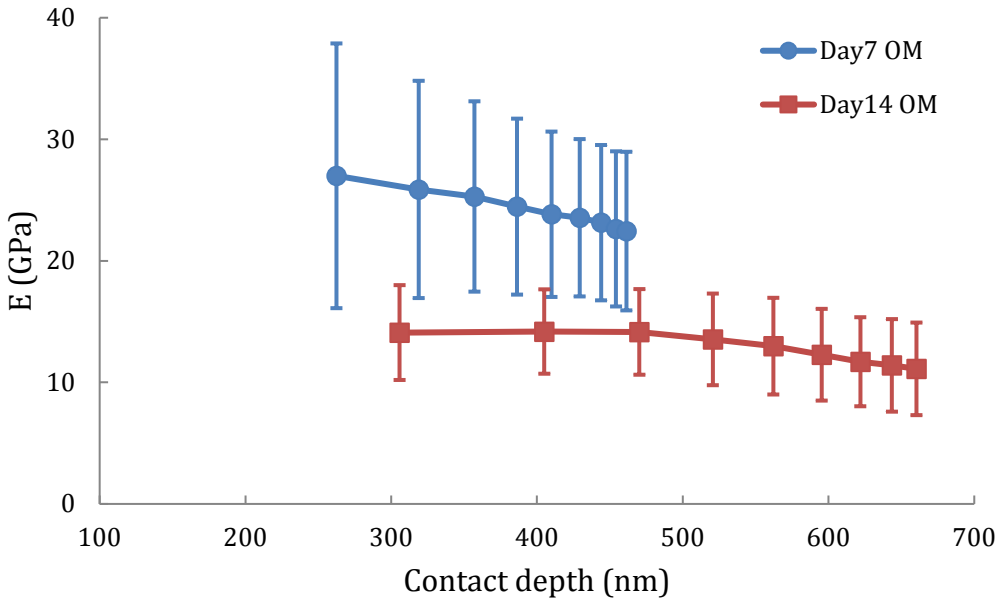

(b)

Fig.4. Young's modulus (± SD) of samples cultured in (a) BM and (b) OM ($p<0.001$), as a function of average contact depth for nanoindentation tests in the peak load range 1-9 mN.

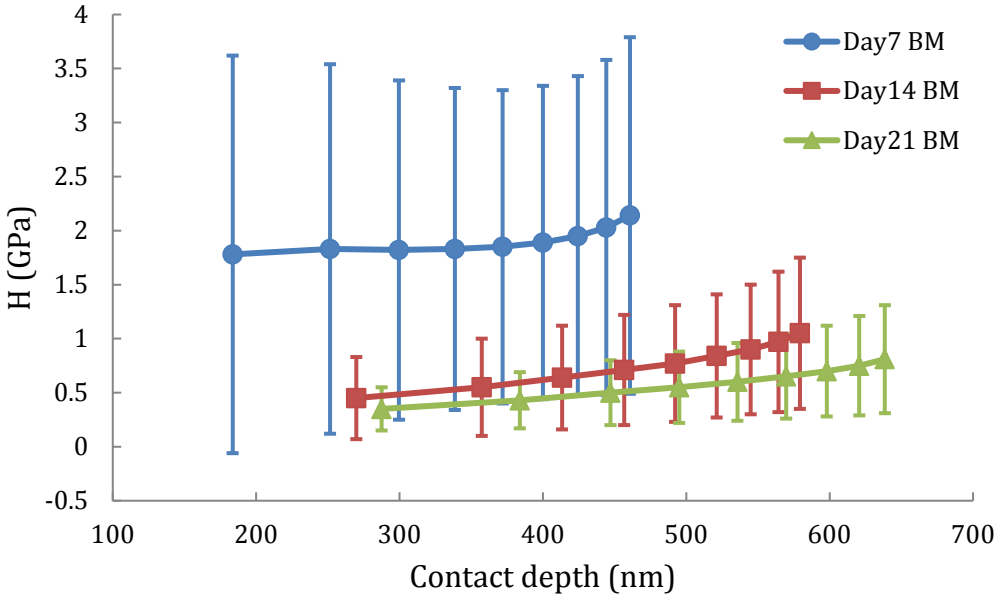

(a)

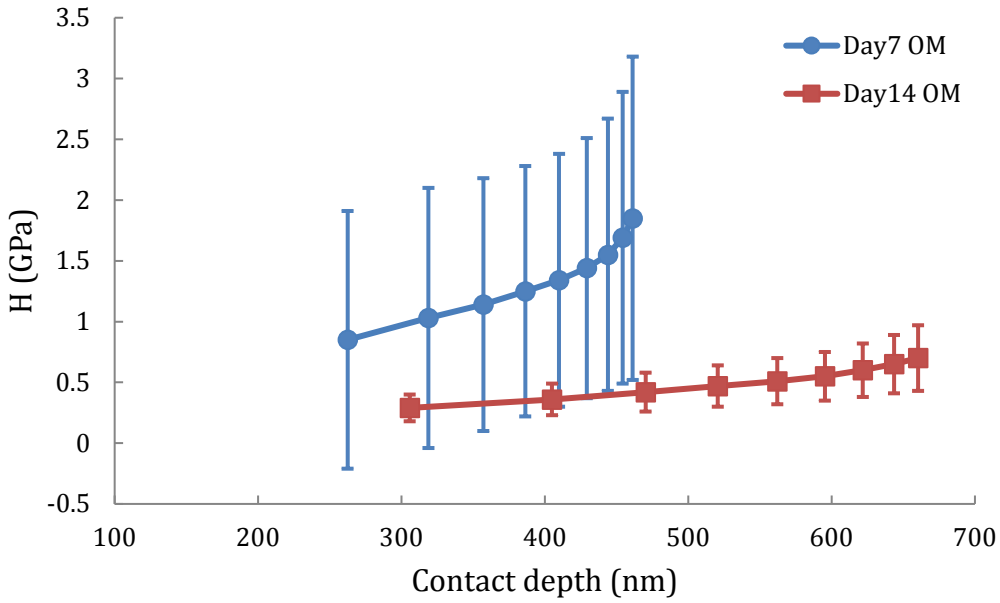

(b)

Fig.5. Hardness (± SD) of samples cultured in (a) BM and (b) OM ($p<0.001$), as a function of average contact depth for nanoindentation tests in the peak load range 1-9 mN.

It is also interesting to investigate the distribution of the measured apparent elastic modulus. It was reported elsewhere that the engineered bone can have a wide distribution of nanoindentation modulus [15, 16]. For example, Fig.6 shows the distribution of the nanoindentation modulus for an engineered bone produced by the C3H10T1/2 MSC line grown in vivo for 28 days [15]. For comparison, Fig.7 displays histograms of elastic modulus for mineralized matrix samples at the same peak loads (*i.e.* 1000 μN and 7000 μN). Similar to the data shown in Fig.6, the distribution of modulus for all the BM samples shown in Fig.7 also presents a multimodal distribution at lower peak loads, and a homogenized response at higher peak loads (with comparable peak modulus values). This may suggest that the mineralized matrix produced by Y201 MSCs is similar to mature bone matrix produced by C3H10T1/2 MSCs. For samples cultured in the OM, this multimodal distribution can only be observed on day 7. The measured Young's modulus decreases from day 7 to day 14, but the variation of the Young's modulus is relatively stable with the change of the indentation force. This may suggest that the matrix cultured from the OM is more uniform than the matrix cultured from the BM, just like the collagen fibre distribution shown in the previous polarized light images (Fig.3).

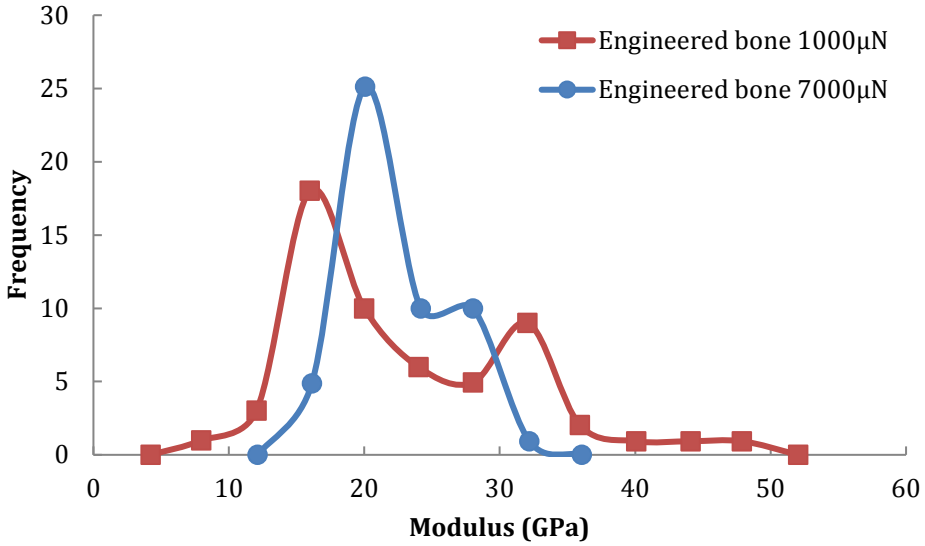

Fig.6. Histograms of elastic modulus for reported engineered bone produced by C3H10T1/2 MSC line grown in vivo for 28 days [15].

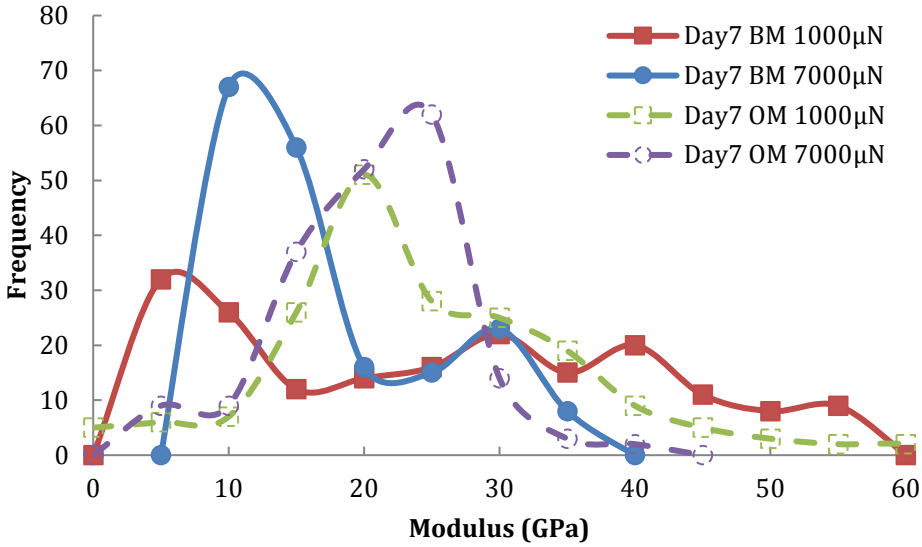

(a)

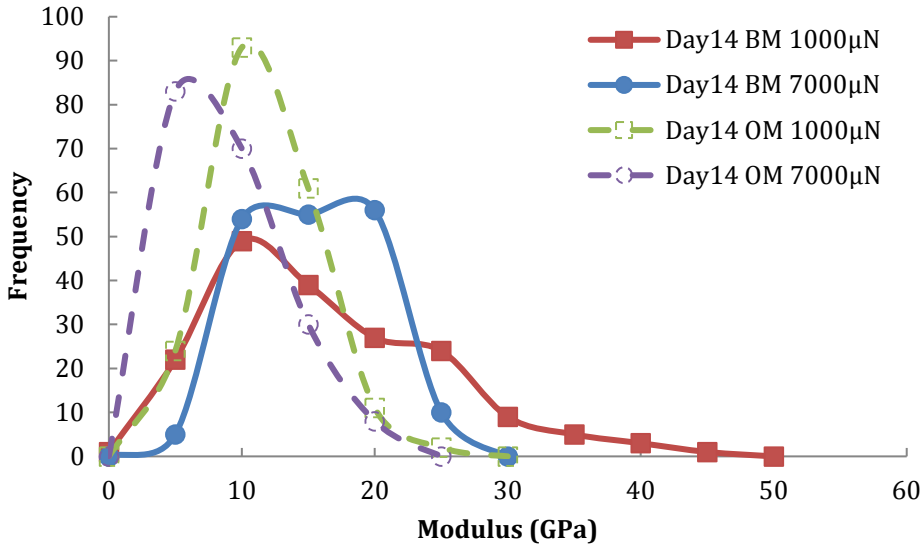

(b)

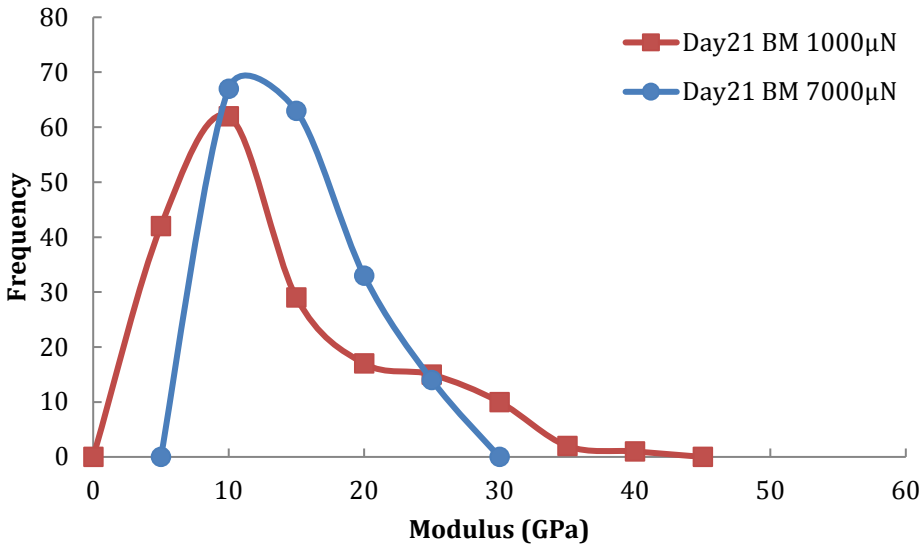

(c)

Fig.7. Histograms of elastic modulus for mineralized matrix samples cultured from (a) day 7, (b) day 14 and (c) day 21, tested at two different peak loads (1000 μN and 7000 μN).

In the given load range (1-9 mN), the average hardness of samples cultured in the BM varies between 1.78-2.14 GPa at day 7. These values decrease to 0.45-1.05 GPa at day 14 and 0.35-0.81 GPa at day 21. The average hardness of samples cultured in the OM varies between 0.85-1.85 GPa at day 7 and then decreases to 0.29-0.70 GPa at day 14. This shows that, in the same period, the hardness of the matrix from BM is greater than that from OM. For both BM and OM, the hardness of the matrix decreases with increasing culture period, and the values (both hardness and SD) from day 7 are much bigger than values from day 14 and day 21. This may indicate that the matrix from day 7 is relatively thin and highly affected by the substrate, and the corresponding collagen fibres are not yet well aligned. The measured hardness values

at day 7 (both BM and OM) are much more scattered compared to the rest of the samples. This may suggest that the hardness of the matrix at day 7 is highly affected by its porous heterogeneous structure. It has been reported that the hardness of canine cortical bone in nanoindentation is 0.638±0.152 GPa within Haversian systems or 0.792±0.144 GPa within non-Haversian areas [49], and the hardness of human cortical bone is 0.85±0.45 GPa measured by a multi-cycling test [50]. This indicates that, compared to the hardness of cortical bone, the matrix cultured in both BM and OM for 7 days is relatively stiff, and the matrix cultured in both BM and OM for 14 and 21 days is more similar to native bone.

3.2.2 Data analysis by the Gaussian mixture model

The structure and composition of biological tissues are often complex, which leads to a complicated mechanical response in a nanoindentation test [51-53]. It has been reported that the Young's modulus of cortical bone is anisotropic [48, 54]. For dehydrated human tibial cortical bone, the elastic modulus of osteogenic lamellae measured by nanoindentation is 14-19 GPa in the transverse direction, and 23-27 GPa in the longitudinal direction. The elastic modulus of interstitial lamellae is 17-21 GPa in the transverse direction, and 25-29 GPa in the longitudinal direction [55]. Thus, the mineralized matrix may also be anisotropic like the bone tissue.

Fig.8 depicts the representative distributions of Young's modulus for the matrix harvested from BM and OM after 14 days, tested at a peak load of 1000 μN. Similar to our previous study, the Gaussian mixture model enables us to extract two components of the nanoindentation modulus and hardness for the matrix in BM and OM (as shown in Fig.9 and Fig.10). For samples cultured in BM, the Young's modulus of component 1 is approximately 10-17 GPa, which seems almost independent of cell culture period. The Young's modulus of component 2 is approximately 28-34 GPa at day 7, and after day 7, this value decreases to 20-25 GPa. The hardness of component 1 is about 0.3-0.7 GPa, and is also almost independent of culture period. The hardness of component 2 is 2.52-2.84 GPa at day 7, this value decreases to 0.97-1.75 GPa at day 14, and further decreases to 0.6-1.27 GPa at day 21. For samples cultured in the OM, it seems that the elastic modulus and hardness are dependent on the cell culture period. From day 7 to day 14, the elastic modulus of component 1 decreases from 21.6-23.7 GPa to 7.8-11.4 GPa, and the elastic modulus of component 2 decreases from 22.8-28.4 GPa to 13.4-19.6 GPa. The hardness of component 1 decreases from 0.42-1.15 GPa to 0.24-0.57 GPa, and the hardness of component 2 decreases from 2.04-2.96 GPa to 0.39-0.90 GPa in the same period. To further investigate the aging and culture medium effects on the mechanical properties, the mean values

of Young's modulus and hardness of each component are taken across the entire contact depth range, which is shown in Fig.11. For samples cultured in the BM, both the Young's modulus and hardness values of component 1 are almost independent of culture period, but those of component 2 decrease with increasing culture period. For samples cultured in OM, both the Young's modulus and hardness of each component decrease from day 7 to day 14. It has been reported that a high seeding density (higher than 5000 cells/cm2) will lead to the detachment of the cell layers between day 12 and day 16 [56]. Thus, according to the seeding density in this study (15000 cells/cm2), the decrease of the stiffness and hardness is probably due to the fact that the early stage of cell detachment occurs before day 14.

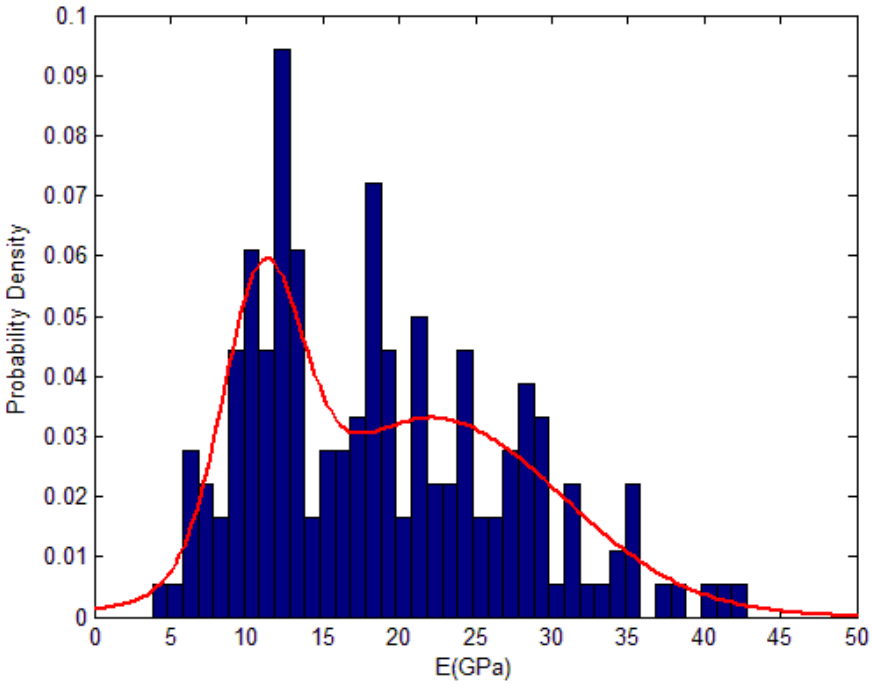

(a)

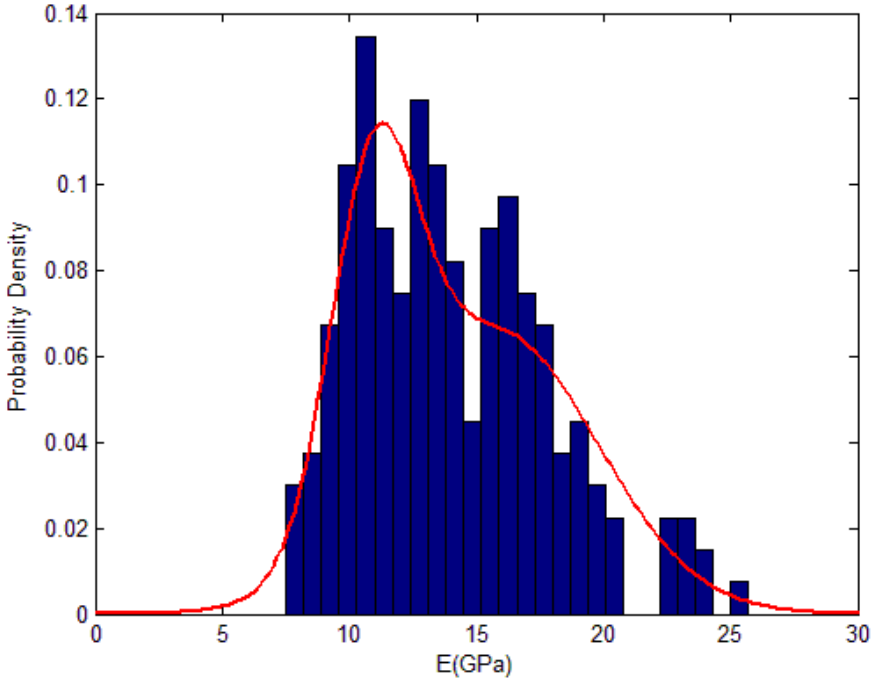

(b)

Fig.8. Representative distributions of Young's modulus for the matrix harvested from (a) day 14, BM, (b) day 14, OM, tested at a peak load of 1000 μN.

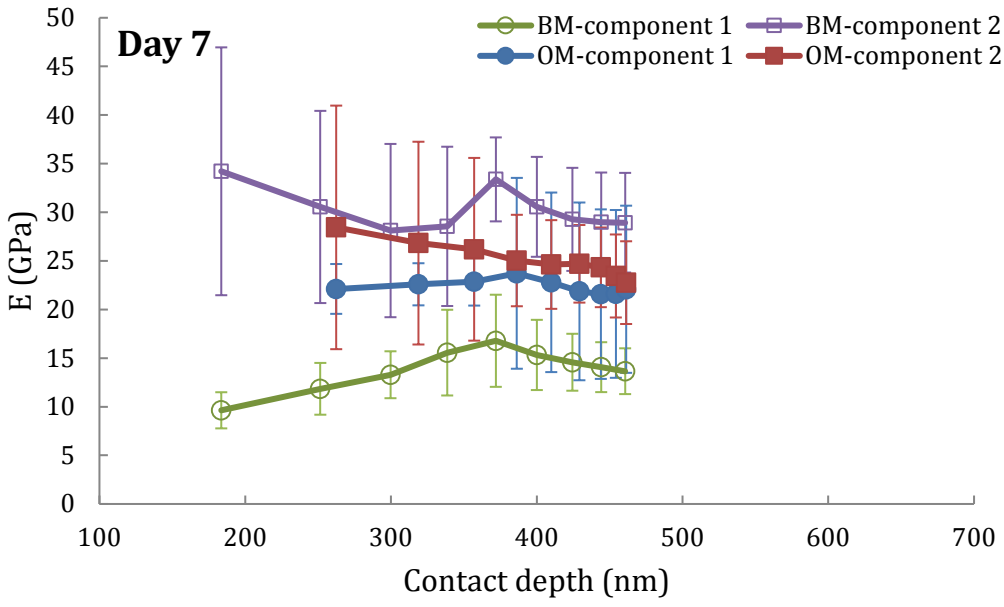

(a)

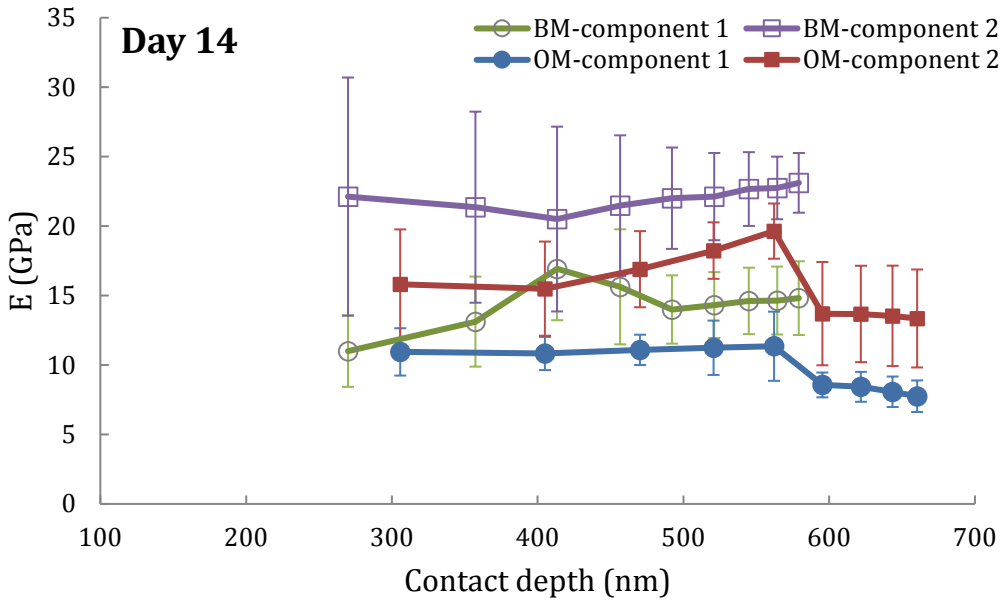

(b)

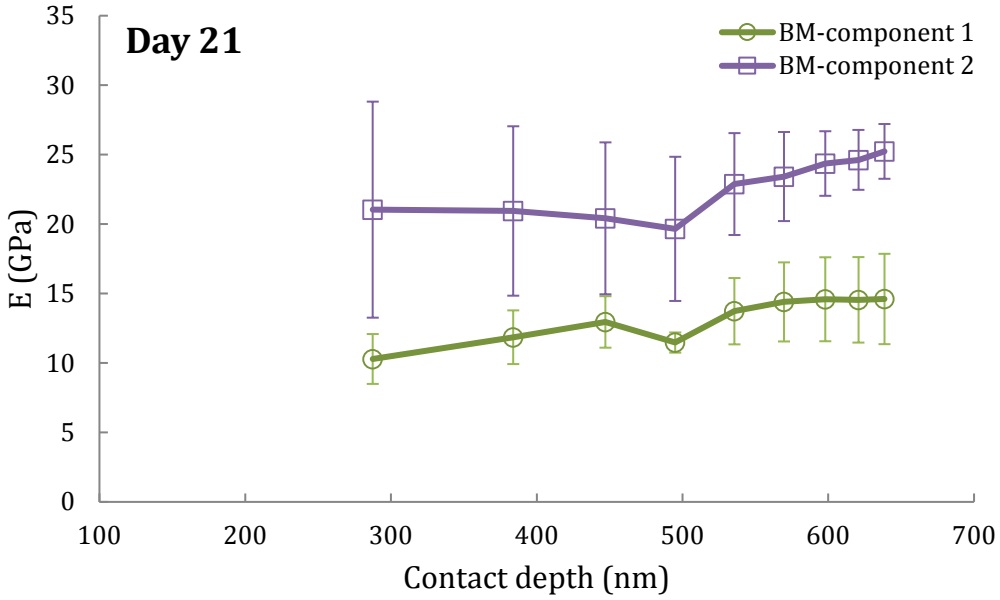

(c)

Fig.9. Young's modulus of two different components in the matrix cultured in different media for (a) 7 days, (b) 14 days and (c) 21 days determined by the Gaussian mixture model for nanoindentation tests in the peak load range 1-9 mN.

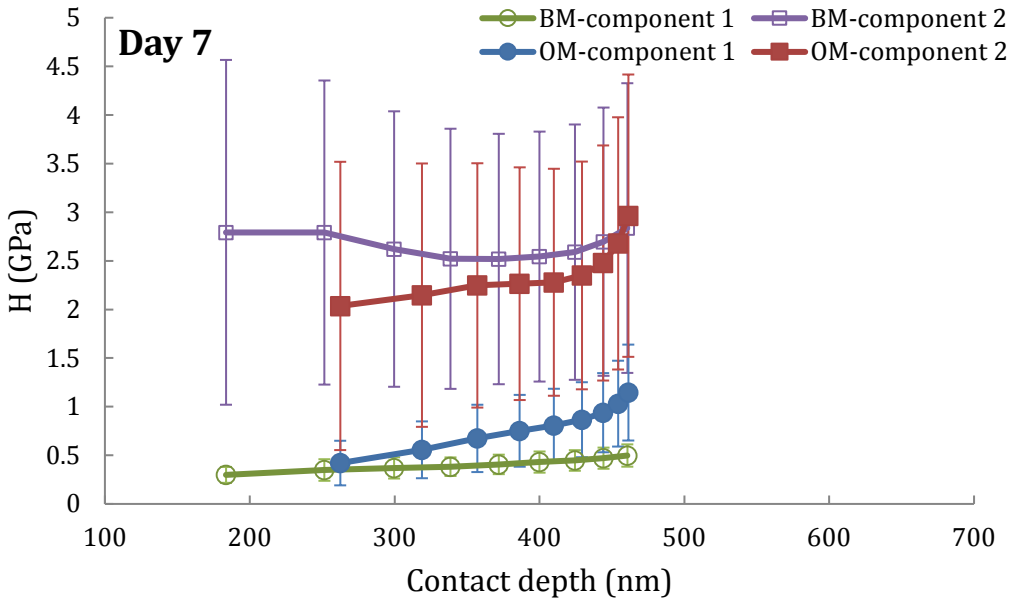
Day 7
BM-component 1
BM-component 2
OM-component 1
OM-component 2
H (GPa)
Contact depth (nm)
0
0.5
1
1.5
2
2.5
3
3.5
4
4.5
5
100
200
300
400
500
600
700

(a)

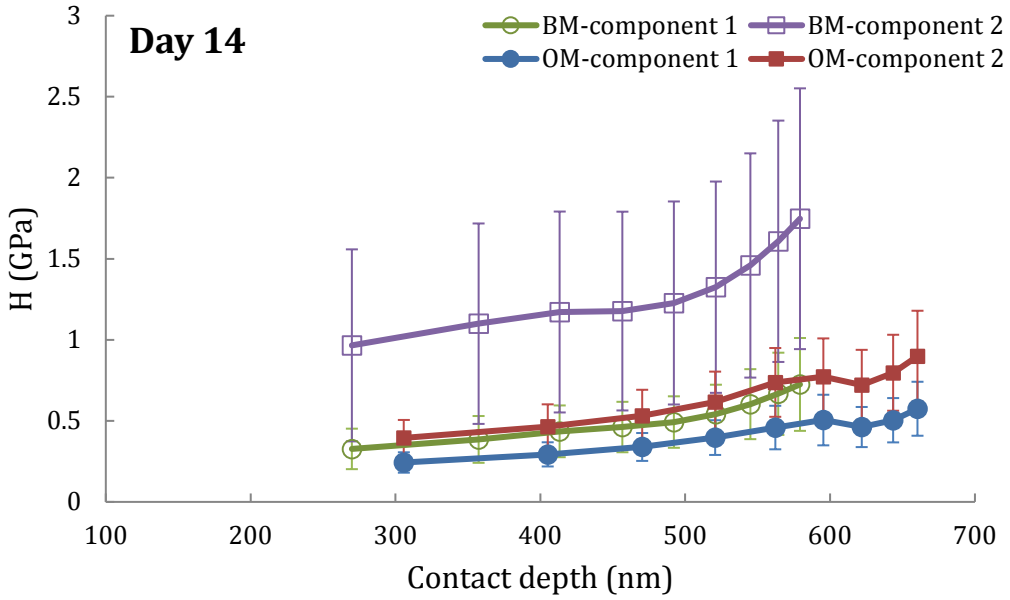
Day 14
BM-component 1
BM-component 2
OM-component 1
OM-component 2
H (GPa)
Contact depth (nm)
0
0.5
1
1.5
2
2.5
3
100
200
300
400
500
600
700

(b)

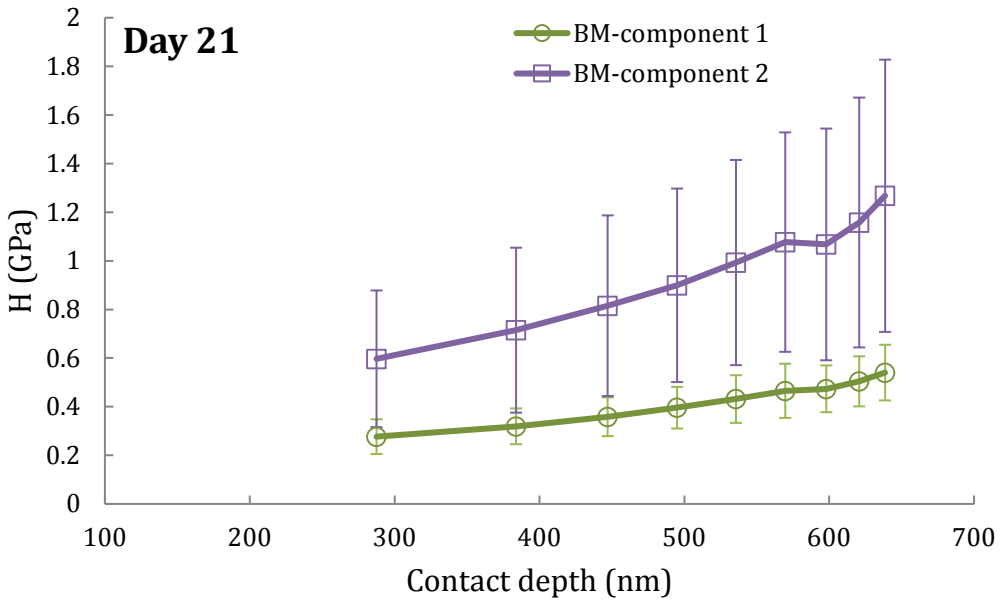

(c)

Fig.10. Hardness of two different components in the matrix cultured in different media for (a) 7 days, (b) 14 days and (c) 21 days, determined by the Gaussian mixture model for nanoindentation tests in the peak load range 1-9 mN.

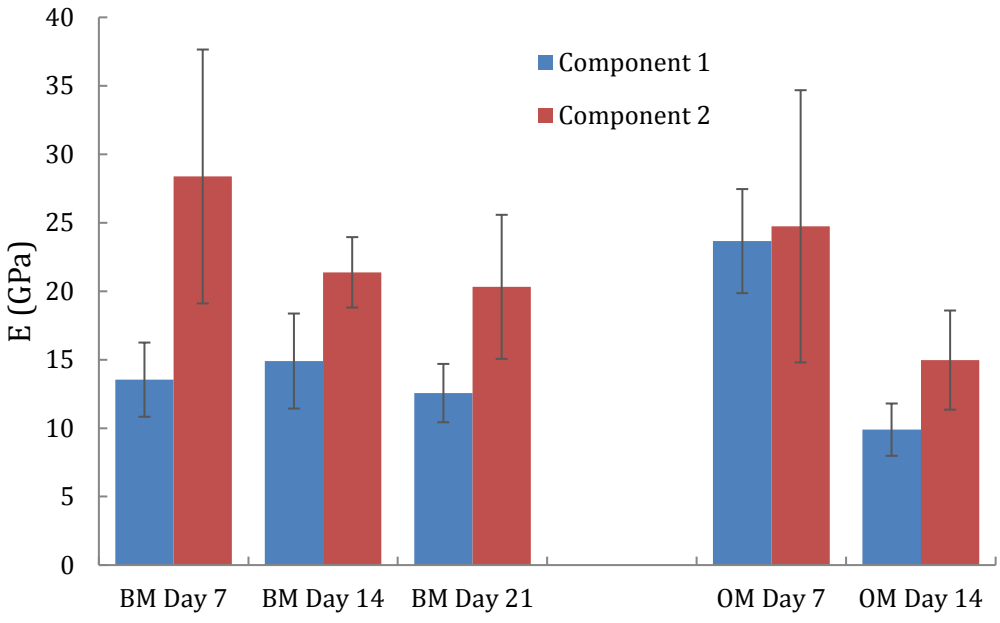

(a)

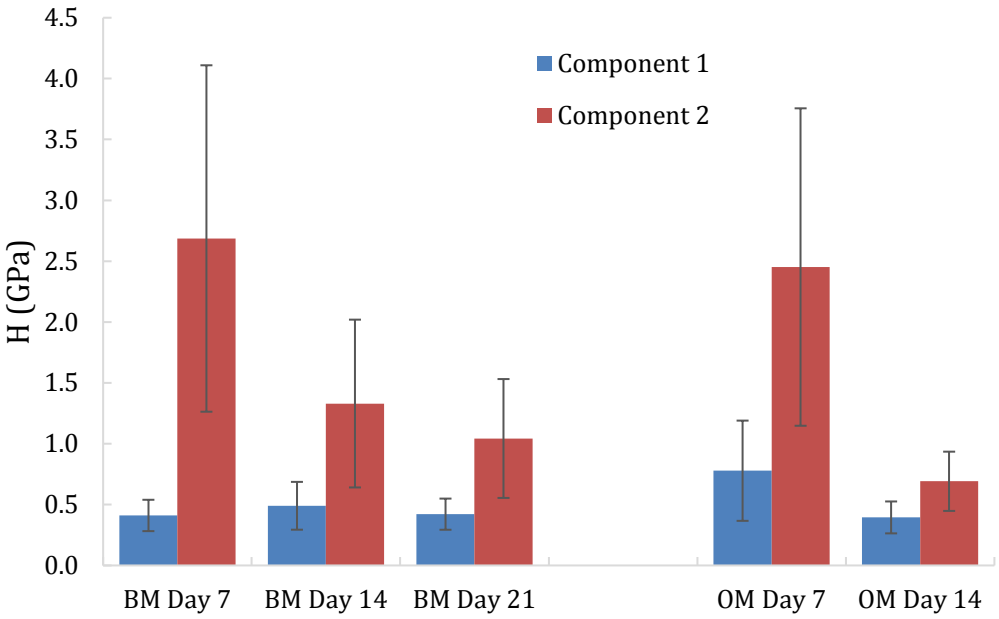

(b)

Fig.11. (a) The Young's modulus and (b) hardness of each component in the matrix cultured in different media as a function of culture period.

From this simple analysis it is not possible to determine the cause of these differences in properties; the two components can be due to the elastic modulus mismatch in the longitudinal and transverse directions (*i.e.* transverse isotropy) or it may also be attributed to the two components with different mechanical properties. For native bone, the transversely isotropic properties can be evident in various native strain regions (such as compressive strain region, tensile strain region and the neutral axis of bending) [57]. If we assume that a similar transverse characteristic is also presented in the mineralized matrix, we could investigate its anisotropy ratio to determine if this is a suitable explanation. Fig.12 illustrates the anisotropy ratio of elastic modulus and hardness between component 1 and component 2 for different samples, as a function of peak loading force. In Fig.12a, a higher elastic anisotropy ratio can be observed at day 7 for samples cultured in BM (especially when contact depth is smaller than approximately 250 nm), and in Fig.12b, the ratio is much lower on day 7 for samples cultured in OM. As shown in Fig.12c and Fig.12d, the anisotropy ratio of hardness and its variation at day 7, which is dependent on the average contact depth, is much greater than values at day 14 and day 21. After day 14, the anisotropy ratio of hardness becomes independent of the average contact depth, with the value changing between 2.2-3.0 for samples cultured in BM and 1.5-1.6 for samples cultured in OM. These observations agree with the previous polarized light results (Fig.3), namely, the matrix cultured from the OM is more uniform than the matrix cultured from the BM. Moreover, it has been reported that the elastic anisotropy ratio of human vertebral

trabeculae is 1.18-1.27 [47], and the ratio for bone tissue from the canine radius of the adult foxhound is 1.334±0.007, and this value reduces to 1.141±0.029 after demineralization or increases to 1.658±0.107 after deproteinization [57]. This indicates that, after 7 to 14 days, the elastic anisotropy ratios of the samples (cultured in both BM and OM) are similar to those from native bone. The relatively high elastic anisotropy ratio of samples cultured in BM for 7 days may result from both the porous surface at small contact depths and the lower protein content in the sample. In contrast, the anisotropy of properties of mineralized matrix cultured in OM is not clear until day 14. The two components are relatively compliant, which may indicate that OM promotes cell proliferation rather than mineralization.

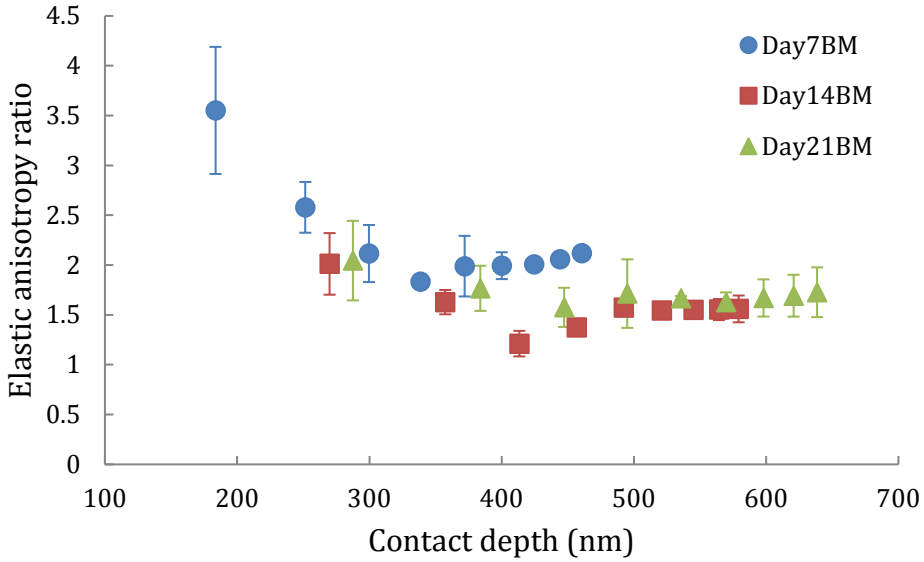

(a)

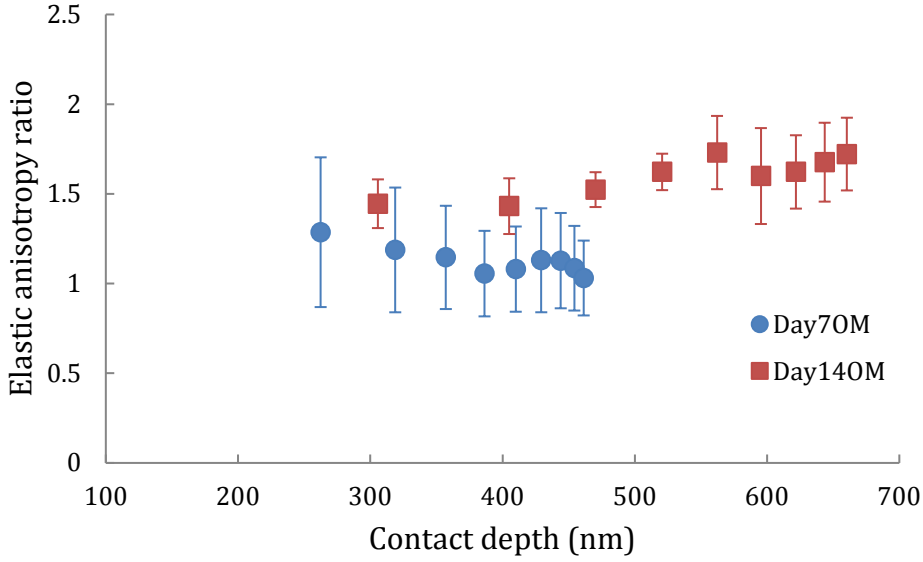

(b)

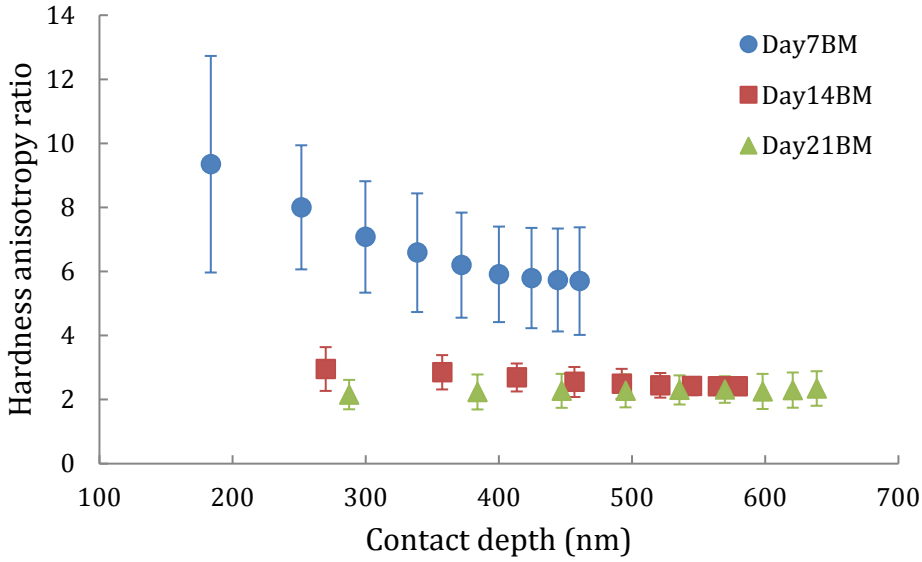

(c)

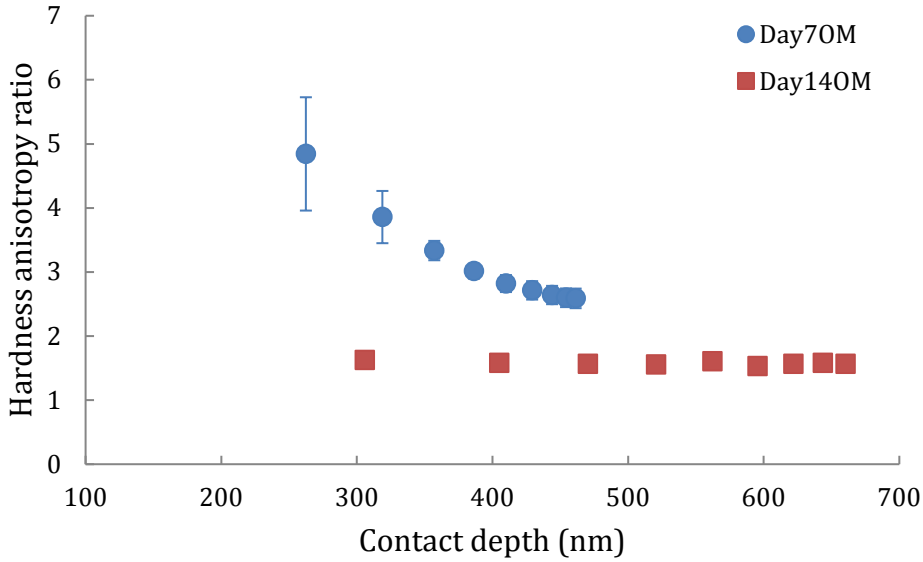

(d)

Fig.12. The depth dependent elastic anisotropy ratio for samples cultured in (a) BM and (b) OM, and hardness anisotropic ratio for samples cultured in (c) BM and (d) OM, as a function of contact depth for nanoindentation tests in the peak load range 1-9 mN.

3.3 Finite element simulations

In addition to being transversely isotropic as the native bone is, the mineralized matrix may also be composed of two components with different properties, which represent the mature and immature bone nodules. In order to identify which of these two situations is most likely using a theoretical approach, FE simulations were performed to simulate the nanoindentation in these two cases. The elastic moduli of the numerical model indented at different locations (as illustrated in Fig.1) around the interface are shown in Fig.13, as a function of indentation depth. The Oliver and Pharr method to extract mechanical properties from load-displacement data

slightly overestimates the modulus obtained from the FEA results for anisotropic materials [39, 40]. From a qualitative perspective, it can be seen that transversely isotropic and two-component assumptions lead to similar pattern of the nanoindentation modulus variation with indentation penetration. With reducing the distance between the indentation point and the interface (point E), the effect from the other part is increasing. A multimodal distribution of elastic modulus for mineralized matrix can be observed at lower indentation depth. By contrast, this elastic modulus is scattered and reaches the equilibrium value at larger indentation depth. The values obtained at the same penetrations and locations for both cases are very similar with a deviation between 5-12%. For both cases, the distribution of the apparent nanoindentation modulus is not as wide as that observed in the experimental measurements.

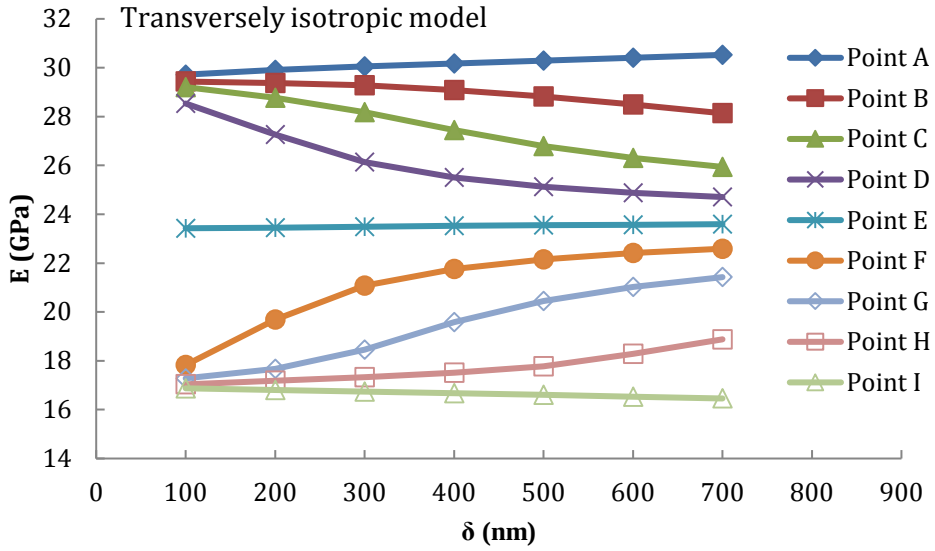

(a)

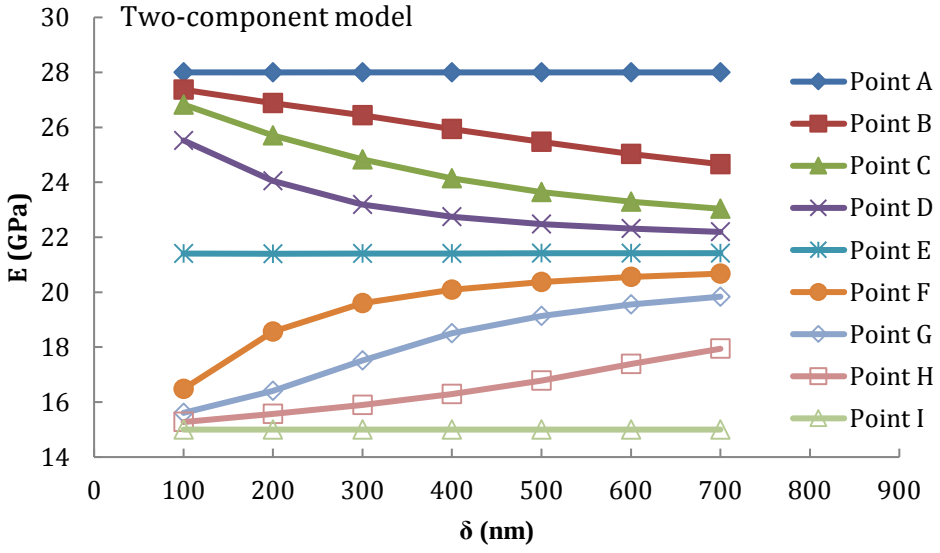

(b)

Fig.13. The elastic modulus of the numerical model indented at different locations (as illustrated in Fig.1) around the interface between (a) two orthogonal fibres, and (b) mature

and immature bone nodules.

4. Conclusions

In this study, the nanoindentation with multi-cycling protocol proved to be effective to study how the nanomechanical properties of the matrix synthesized by the cell would be affected by cell culture media and culture duration. Together with surface analysis and FEA, the correlation between the sample microstructure and nanomechanics has been studied.

Nanoindentation tests have revealed that the stiffness and hardness of bone nodules (*i.e.* mineralized matrix) produced by Y201 cell line are comparable to native bone, and present a multimodal distribution. As an explanation, these bone nodules may present both mature (stiff phase) and immature (compliant phase) state. However, there is no direct evidence to support this assumption. As another explanation, similar to native bone, the multimodal distribution is more likely due to the anisotropic behaviour of these bone nodules, which has been revealed in the polarized light images. The ratio of elastic modulus and hardness at these two orthogonal directions (or between stiffer and softer phases) can be up to 2 and 5, respectively. The bone nodules produced by cells in basal medium appear to be stiffer and more anisotropic compared to that in osteogenic medium, as confirmed in both nanoindentation tests and polarized light images. In the polarized light images, an anisotropic collagen fibre distribution has been observed on BM samples and a relatively uniform collagen fibre distribution has been observed on their counterparts from OM. This anisotropic collagen fibre distribution explains the multimodal distribution of the mechanical properties, as confirmed in the FE simulations.

From the point of culture period, it has also been shown that the cell culture duration does not affect the elastic modulus and hardness in the transverse direction but it significantly affects the elastic modulus and hardness at longitudinal direction after day 7. When cell culture period reaches 14 days, the matrix becomes stabilized in the longitudinal direction and there is no further change with the cell culture period. In addition, mineralized matrix has revealed a more porous structure at day 7, compared to that at day 14 and 21, which explains the wider span of the distribution of measured mechanical properties at day 7. For both basal and osteogenic media, the bone nodules have exhibited reverse aging behaviour compared to native bone. This is possibly due to the fact that cell proliferation outcompetes the mineralization process.

Acknowledgments

P. Duan acknowledges Newcastle University for providing a studentship. J. Chen is acknowledging funding from the Engineering and Physical Sciences Research Council

(EP/K039083/1). In addition, Dr. Himadri Gupta and Prof. Yanping Cao are also acknowledged for useful discussions.

References

1. Stevens, M.M., *Biomaterials for bone tissue engineering.* Materials Today, 2008. **11**(5): p. 18-25.
2. Ferreira, A.M., et al., *Collagen for bone tissue regeneration.* Acta Biomaterialia, 2012. **8**(9): p. 3191-3200.
3. Baino, F., et al., *Optimization of composition, structure and mechanical strength of bioactive 3-D glass-ceramic scaffolds for bone substitution.* Journal of Biomaterials Applications, 2011: p. 0885328211429193.
4. Deb, S., R. Mandegaran, and L. Di Silvio, *A porous scaffold for bone tissue engineering/45S5 Bioglass® derived porous scaffolds for co-culturing osteoblasts and endothelial cells.* Journal of Materials Science: Materials in Medicine, 2010. **21**(3): p. 893-905.
5. Zhang, H., X.-J. Ye, and J.-S. Li, *Preparation and biocompatibility evaluation of apatite/wollastonite-derived porous bioactive glass ceramic scaffolds.* Biomedical Materials, 2009. **4**(4): p. 045007.
6. Tuan, R.S., G. Boland, and R. Tuli, *Adult mesenchymal stem cells and cell-based tissue engineering.* Arthritis Research and Therapy, 2003. **5**(1): p. 32-45.
7. Gamie, Z., et al., *Stem cells combined with bone graft substitutes in skeletal tissue engineering.* Expert Opinion on Biological Therapy, 2012. **12**(6): p. 713-729.
8. Bianco, P. and P.G. Robey, *Stem cells in tissue engineering.* Nature, 2001. **414**(6859): p. 118-121.
9. James, S., et al., *Multiparameter analysis of human bone marrow stromal cells identifies distinct immunomodulatory and differentiation-competent subtypes.* Stem Cell Reports, 2015. **4**(6): p. 1004-1015.
10. Gong, M., et al., *Immortalized mesenchymal stem cells: an alternative to primary mesenchymal stem cells in neuronal differentiation and neuroregeneration associated studies.* Journal of Biomedical Science, 2011. **18**(1): p. 1.
11. Liu, T.M., et al., *Molecular basis of immortalization of human mesenchymal stem cells by combination of p53 knockdown and human telomerase reverse transcriptase overexpression.* Stem Cells and Development, 2012. **22**(2): p. 268-278.
12. Gough, J.E., J.R. Jones, and L.L. Hench, *Nodule formation and mineralisation of human primary osteoblasts cultured on a porous bioactive glass scaffold.* Biomaterials, 2004. **25**(11): p. 2039-2046.
13. Bandyopadhyay‐Ghosh, S., et al., *Osteoconductivity of modified fluorcanasite*

glass‐ceramics for bone tissue augmentation and repair. Journal of Biomedical Materials Research Part A, 2010. **94**(3): p. 760-768.

14. Jell, G., et al., *Bioactive glass‐induced osteoblast differentiation: A noninvasive spectroscopic study.* Journal of Biomedical Materials Research Part A, 2008. **86**(1): p. 31-40.
15. Pelled, G., et al., *Structural and nanoindentation studies of stem cell-based tissue-engineered bone.* J Biomech, 2007. **40**(2): p. 399-411.
16. Chen, J., M.A. Birch, and S.J. Bull, *Nanomechanical characterization of tissue engineered bone grown on titanium alloy in vitro.* J Mater Sci Mater Med, 2010. **21**(1): p. 277-82.
17. Jang, I.K., et al., *Nanomechanical properties and molecular structures of in vitro mineralized tissues on anodically-oxidized titanium surfaces.* Nanomedicine, 2014. **10**(3): p. 629-37.
18. Tai, K., et al., *Nanobiomechanics of repair bone regenerated by genetically modified mesenchymal stem cells.* Tissue Eng Part A, 2008. **14**(10): p. 1709-20.
19. Kavukcuoglu, N.B., P. Patterson-Buckendahl, and A.B. Mann, *Effect of osteocalcin deficiency on the nanomechanics and chemistry of mouse bones.* J Mech Behav Biomed Mater, 2009. **2**(4): p. 348-54.
20. Kavukcuoglu, N.B., et al., *Osteopontin deficiency and aging on nanomechanics of mouse bone.* J Biomed Mater Res A, 2007. **83**(1): p. 136-44.
21. Oyen, M.L., *Nanoindentation of hydrated materials and tissues.* Current Opinion in Solid State and Materials Science, 2015. **19**(6): p. 317-323.
22. Li, X., et al., *Microindentation test for assessing the mechanical properties of cartilaginous tissues.* Journal of Biomedical Materials Research Part B: Applied Biomaterials, 2007. **80**(1): p. 25-31.
23. Duan, P. and J. Chen, *Nanomechanical and microstructure analysis of extracellular matrix layer of immortalized cell line Y201 from human mesenchymal stem cells.* Surface and Coatings Technology, 2015. **284**: p. 417-421.
24. Burstein, A.H., D.T. Reilly, and M. Martens, *Aging of bone tissue: mechanical properties.* J Bone Joint Surg Am, 1976. **58**(1): p. 82-86.
25. Zioupos, P., J.D. Currey, and A.J. Hamer, *The role of collagen in the declining mechanical properties of aging human cortical bone.* Journal of Biomedical Materials Research, 1999. **45**(2): p. 108-116.
26. Zioupos, P. and J.D. Currey, *Changes in the stiffness, strength, and toughness of human*

cortical bone with age. Bone, 1998. **22**(1): p. 57-66.

27. Langenbach, F. and J. Handschel, *Effects of dexamethasone, ascorbic acid and β-glycerophosphate on the osteogenic differentiation of stem cells in vitro.* Stem Cell Res Ther, 2013. **4**(5): p. 117.
28. Seo, C.H., et al., *Micropit surfaces designed for accelerating osteogenic differentiation of murine mesenchymal stem cells via enhancing focal adhesion and actin polymerization.* Biomaterials, 2014. **35**(7): p. 2245-2252.
29. Kim, K.-I., S. Park, and G.-I. Im, *Osteogenic differentiation and angiogenesis with cocultured adipose-derived stromal cells and bone marrow stromal cells.* Biomaterials, 2014. **35**(17): p. 4792-4804.
30. Ferreira, A.M., et al., *Bone Collagen Role in Piezoelectric Mediated Remineralization.* Acta Microscopica, 2009. **18**(3).
31. Whittaker, P., et al., *Quantitative assessment of myocardial collagen with picrosirius red staining and circularly polarized light.* Basic Research in Cardiology, 1994. **89**(5): p. 397-410.
32. Rosenbloom, J., W.R. Abrams, and R. Mecham, *Extracellular matrix 4: the elastic fiber.* The FASEB Journal, 1993. **7**(13): p. 1208-1218.
33. Hillmann, G. and W. Geurtsen, *Light-microscopical investigation of the distribution of extracellular matrix molecules and calcifications in human dental pulps of various ages.* Cell and Tissue Research, 1997. **289**(1): p. 145-154.
34. Martin, R.B. and J. Ishida, *The relative effects of collagen fiber orientation, porosity, density, and mineralization on bone strength.* Journal of Biomechanics, 1989. **22**(5): p. 419-426.
35. Bromage, T.G., et al., *Circularly polarized light standards for investigations of collagen fiber orientation in bone.* The Anatomical Record, 2003. **274**(1): p. 157-168.
36. Doillon, C.J., et al., *Collagen fiber formation in repair tissue: development of strength and toughness.* Collagen and Related Research, 1985. **5**(6): p. 481-492.
37. Chen, J. and S.J. Bull, *Multi-cycling nanoindentation study on thin optical coatings on glass.* Journal of Physics D: Applied Physics, 2008. **41**(7): p. 074009.
38. Oliver, W.C. and G.M. Pharr, *An improved technique for determining hardness and elastic modulus using load and displacement sensing indentation experiments.* Journal of Materials Research, 1992. **7**(06): p. 1564-1583.
39. Fan, Z., J.Y. Rho, and J.G. Swadener, *Three-dimensional finite element analysis of the*

effects of anisotropy on bone mechanical properties measured by nanoindentation. Journal of Materials Research, 2004. **19**(01): p. 114-123.

40. Carnelli, D., et al., *Nanoindentation testing and finite element simulations of cortical bone allowing for anisotropic elastic and inelastic mechanical response.* Journal of Biomechanics, 2011. **44**(10): p. 1852-1858.
41. Zaichick, V. and M. Tzaphlidou, *Calcium and phosphorus concentrations and the calcium/phosphorus ratio in trabecular bone from the femoral neck of healthy humans as determined by neutron activation analysis.* Applied Radiation and Isotopes, 2003. **58**(6): p. 623-627.
42. Donzelli, E., et al., *Mesenchymal stem cells cultured on a collagen scaffold: In vitro osteogenic differentiation.* Archives of Oral Biology, 2007. **52**(1): p. 64-73.
43. Gronthos, S., et al., *The STRO-1+ fraction of adult human bone marrow contains the.* Blood, 1994. **84**(12): p. 4164-4173.
44. Stylianou, A., et al., *AFM multimode imaging and nanoindetation method for assessing collagen nanoscale thin films heterogeneity.* XIII Mediterranean Conference on Medical and Biological Engineering and Computing 2013, 2014: p. 407-410.
45. Chaudhry, B., et al., *Nanoscale viscoelastic properties of an aligned collagen scaffold.* Journal of Materials Science: Materials in Medicine, 2009. **20**(1): p. 257-263.
46. Wu, Y.D., et al., *Granulocyte colony‐stimulating factor administration alters femoral biomechanical properties in C57BL/6 mice.* Journal of Biomedical Materials Research Part A, 2008. **87**(4): p. 972-979.
47. Wolfram, U., H.-J. Wilke, and P.K. Zysset, *Transverse isotropic elastic properties of vertebral trabecular bone matrix measured using microindentation under dry conditions (effects of age, gender, and vertebral level).* Journal of Mechanics in Medicine and Biology, 2010. **10**(01): p. 139-150.
48. Wenger, M.P.E., et al., *Mechanical properties of collagen fibrils.* Biophysical Journal, 2007. **93**(4): p. 1255-1263.
49. Lin, Z.X., et al., *In situ observation of fracture behavior of canine cortical bone under bending.* Materials Science and Engineering: C, 2016. **62**: p. 361-367.
50. Hoffler, C.E., et al., *An application of nanoindentation technique to measure bone tissue lamellae properties.* Journal of Biomechanical Engineering, 2005. **127**(7): p. 1046-1053.
51. Zebaze, R.M.D., et al., *Differences in the degree of bone tissue mineralization account*

for little of the differences in tissue elastic properties. Bone, 2011. **48**(6): p. 1246-1251.

52. Gupta, H.S., et al., *Nanoscale deformation mechanisms in bone.* Nano Letters, 2005. **5**(10): p. 2108-2111.
53. Gupta, H.S., et al., *Cooperative deformation of mineral and collagen in bone at the nanoscale.* Proceedings of the National Academy of Sciences, 2006. **103**(47): p. 17741-17746.
54. Dong, X.N. and X.E. Guo, *The dependence of transversely isotropic elasticity of human femoral cortical bone on porosity.* Journal of Biomechanics, 2004. **37**(8): p. 1281-1287.
55. Fan, Z., et al., *Anisotropic properties of human tibial cortical bone as measured by nanoindentation.* Journal of Orthopaedic Research, 2002. **20**(4): p. 806-810.
56. Jaiswal, N., et al., *Osteogenic differentiation of purified, culture‐expanded human mesenchymal stem cells in vitro.* Journal of Cellular Biochemistry, 1997. **64**(2): p. 295-312.
57. Takano, Y., et al., *Elastic anisotropy and collagen orientation of osteonal bone are dependent on the mechanical strain distribution.* Journal of Orthopaedic Research, 1999. **17**(1): p. 59-66.